Evolution of Retisol impacted by artificial drainage: What can we learn from stable Fe isotope ratios?

Z Fekiacova, D. Montagne, A. Duvivier, Abel Guihou, P. Deschamps, Sophie S. Cornu

Evolution of Retisol impacted by artificial drainage: What can we learn from stable Fe isotope ratios?

Fekiacova, Z.[1], Montagne, D.[2], Duvivier, A.[1], Guihou, A.[1], Deschamps, P.[1], Cornu, S.[1]

[1] Aix Marseille Univ, CNRS, IRD, INRAE, Coll France, CEREGE, Aix-en-Provence, France

[2] Université Paris-Saclay, INRAE, AgroParisTech, UMR ECOSYS, 78850, Thiverval-Grignon, France.

Abstract

Iron oxides are one of the most reactive mineral phases in soils. As a consequence, their transformations can considerably affect the dynamics of the adsorbed elements and of the associated soil ecosystem services. Understanding the dynamics of Fe oxides in soils is therefore a key issue for the evolution of soil and associated ecosystem services. A potentially powerful tool to study the transformations of Fe-oxides in soil is stable Fe isotopes. However, there are still important gaps in our knowledge of Fe isotope fractionations.

In order to examine the Fe isotope fractionations related to each process occurring in soils, we focused on a drainage-influenced sequence of Retisols, a soil type characterized by clay translocation and subsequent degradation by redox processes inducing a strong spatial Fe segregation in contrasted soil volumes. We combined the isotopic approach at the scale of a bulk horizon and at the scale of the different soil volumes, with mineralogical analyses and mass balance calculations in order to investigate the consequences of the drainage on Fe isotope fractionation. We showed that while there were no Fe isotope fractionations at the profile scale, Fe isotopic signatures varied significantly among soil volumes (δ^{56}Fe values from -0.49 ± 0.05

to 0.29 ± 0.06‰). These variations suggest that redox processes are the main mechanisms responsible for the Fe redistribution among the volumes, and particularly that Fe accumulation during Mn oxide precipitation makes a significant contribution to Fe isotopic fractionation, during these Retisol differentiation. In contrast, drainage-induced eluviation does not result in further Fe isotope fractionations in soil volumes in these Retisols. The isotopic signatures of the different mineral phases present in the volumes were calculated using the mass balance approach and suggest that the iron oxides (goethite, ferrihydrite) have $\delta^{56}Fe$ values close to 0‰, while the clay minerals are enriched in heavy Fe isotopes and the Mn oxides in light Fe isotopes. This study provides insight into the dynamics of Fe minerals in hydromorphic soils and offers a new perspective on stable Fe isotope fractionation in soils.

Keywords: Fe isotopes, redox processes, eluviation, drainage, mineral

Highlights

Dissolution of Fe oxides did not fractionate Fe isotopes during the formation of these Retisols

Precipitation of Mn oxides fractionates Fe isotopes in the studied Retisols

Goethite and ferrihydrite have a Fe isotopic signature close to zero per mill

Clay minerals are enriched in heavy Fe isotopes

Mn oxides are enriched in light Fe isotopes

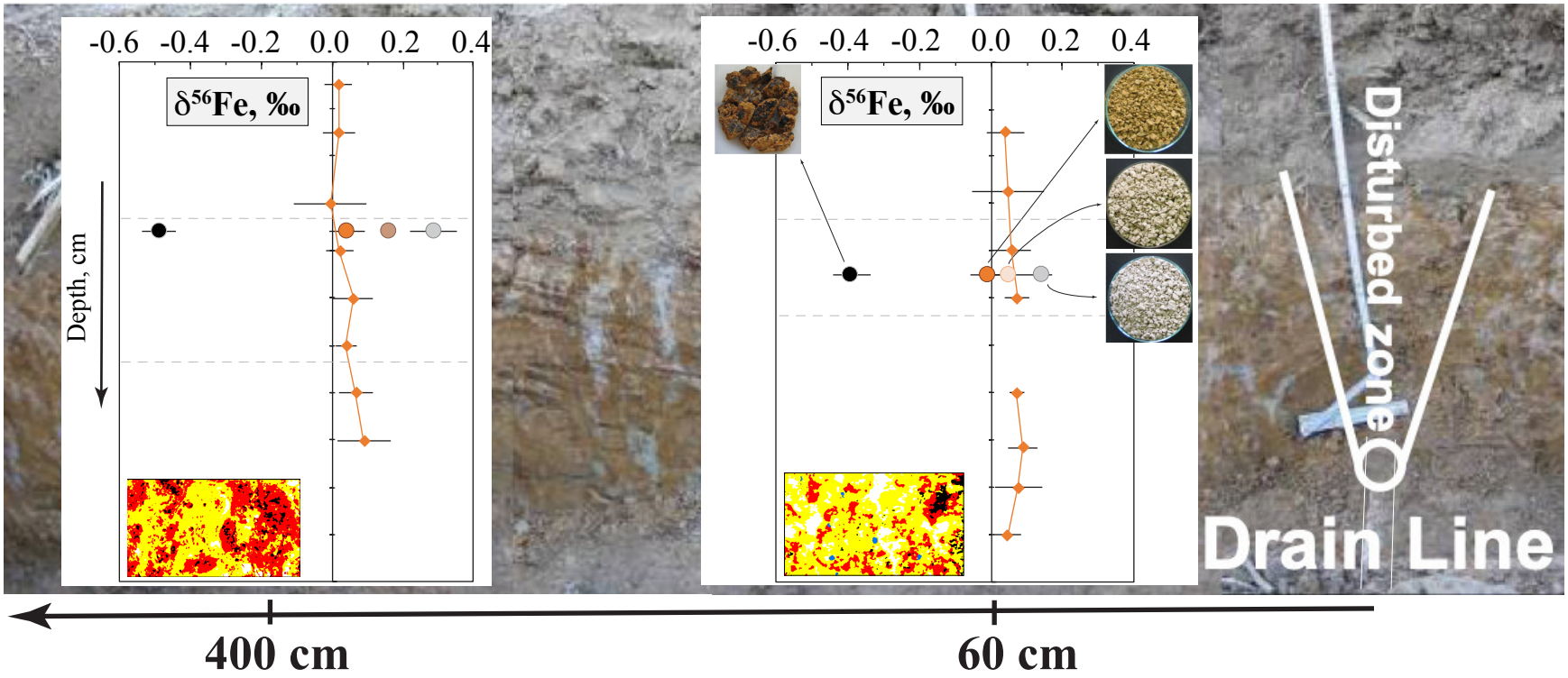

No impact of the drain : natural pedogenesis (redox), Retisol differentiation

Impact of the drain, enhanced eluviation

Graphical Abstract

1. INTRODUCTION

Iron is one of the most dynamic major elements in soils due to its sensitivity to redox conditions. In the form of Fe oxide it also represents one of the most reactive mineral phases in soils (e.g., Cornell and Schwertmann, 2003; Schwertmann, 1991). Elucidating the dynamics of Fe oxides is therefore a key issue for the evolution of soils. A potentially powerful tool to study Fe mineral transformations in soil is the isotopic composition of Fe, as many soil processes (e.g., dissolution, precipitation, lateral and vertical translocation and organic complexation, biological activity such as microbial activity and plant uptake) have been shown to fractionate Fe isotopes. For example, mineral dissolution favors light Fe isotopes in the dissolved fraction (e.g., Beard et al., 1999), colloids with low $\delta^{56}Fe$ values (heavy Fe depleted) play an important role in Fe release from soil (Kusonwiriyawong et al., 2017) and isotopically light Fe is preferentially taken up from the soil Fe pool by strategy I plants, while limited fractionation favoring heavy Fe isotopes was observed during Fe uptake by strategy II plants (e.g., Kiczka et al., 2010; Guelke and von Blanckenburg, 2007). However, there are still significant gaps in our knowledge of Fe isotope fractionations and experimental studies show that the amplitudes and directions of the Fe isotopic fractionations are variable and that their extents can overlap (e.g., Anbar, 2004; Balci et al., 2006; Beard and Johnson 1999; Brantley et al. 2001; Bullen et al., 2001; Icopini et al. 2004; Johnson et al., 2002; Mathews et al., 2001; Skulan et al., 2002). For example, both a rapid non-biological oxidative precipitation of ferrihydrite and a biological extracellular reductive dissolution have been shown to produce a similar range of Fe isotopic fractionations (from ~ -1.5 to -0.5 ‰, Anbar, 2004). The knowledge gaps are even larger when considering processes controlling the isotopic fractionations in natural soils. Despite evident Fe redistributions, the variations of Fe isotopic composition recorded in bulk soil profiles are small ($\Delta^{56}Fe_{profile} \leq 0.15$‰, with $\Delta^{56}Fe_{profile} = \delta^{56}Fe_{max} - \delta^{56}Fe_{min}$ within a given soil profile), with the exception of soils with dominant organic matter-controlled redox processes where $\Delta^{56}Fe_{profile}$

70 can reach up to 0.8 ‰ (e.g., Fekiacova et al., 2017, 2013; Poitrasson et al., 2008; Thompson et
71 al., 2007; Wiederhold et al., 2007a, 2007b). Different hypotheses could explain this apparent
72 contradiction: (i) the soil formation processes do not fractionate Fe isotopes (e.g., a complete
73 dissolution of Fe bearing mineral phases, transport of Fe with the particular phase, etc); (ii) the
74 isotopic fractionations induced by the different soil processes compensate each other; (iii) the
75 mobilization of Fe is too slight (small losses relative to the large stocks) to induce a measurable
76 change in the bulk soil Fe isotopic fractionation.
77 In order to examine the Fe isotope fractionations induced by individual processes in soils,
78 we need to isolate the minerals formed by these processes to analyze their isotopic signatures.
79 However, the available sorting methods commonly used for this purpose in Earth Sciences,
80 namely chemical and physical separations (e.g., Borggaard 1988; Chao and Zhu, 1983;
81 Filgueiras et al., 2002; La Force and Fendorf, 2000) present major drawbacks. Chemical
82 extractions induce an uncontrolled bias in the Fe isotopic composition due to incomplete
83 dissolution of the targeted phase and/or the complexing nature of some of the reagents (e.g.,
84 Wiederhold et al., 2007a). Physical separations are generally not suitable when the size of
85 minerals contained in the soil matrix is very small and are reduced, in the best case, to the
86 analysis of manually isolated soil features, which are indicative of one or a small number of
87 pedological processes. This approach was used by Wiederhold et al. (2007b) who observed a
88 systematic enrichment in light Fe isotopes in the Fe-enriched, and enrichment in heavy Fe
89 isotopes in the Fe-depleted soil features, suggesting a link between pedogenic distribution of
90 Fe and Fe isotopic fractionation.
91 In the present work, in order to elucidate the apparent contradiction between Fe isotope
92 fractionating soil processes and unfractionated bulk soil Fe isotopic profiles, and test the
93 associated hypotheses, we selected a soil sequence characterized by (i) high Fe losses along the
94 soil profile (ii) contrasted redoximorphic features (designated as “soil volumes” hereafter)

95 characterized by strong differences in Fe oxide content and (iii) an pronounced lateral
96 differentiation induced by drainage. The chosen soil sequence consisted of a drainage-
97 influenced sequence of Retisols (IUSS Working Group WRB, 2015) extensively characterized
98 by Montagne et al. (2008). This soil type is characterized by a process of morphological
99 degradation and subsequent clay translocation. The morphological degradation consists in the
100 dissolution of Fe-oxides from the parental ochre material, producing residual pale-brown
101 volumes (PB volumes) and white-grey volumes (WG volumes), and in the precipitation of the
102 released Fe and Mn in black volumes (B volumes) (Cornu et al., 2012a; Montagne et al., 2008).
103 These transformations reflect changes in the mineralogical composition (Montagne et al.,
104 2008). Montagne et al. (2008) demonstrated that drainage of these soils increased the
105 morphological degradation in the vicinity of the drain by enhancing eluviation and decreasing
106 the occurrence of reducing phases (Montagne et al., 2016).
107 We combined the isotopic analyses of soil volumes with mineralogical analyses and mass
108 balance calculations to estimate the Fe isotopic signatures of the different mineral phases. Our
109 aim was to (i) shed light on the fluxes and Fe isotope signatures variability along the soil
110 sequence at three different scales: the horizon, the soil volume and the mineral scale and (ii)
111 decipher the impact of the different soil processes on the Fe isotope signatures.
112
113 ## 2. MATERIAL AND METHODS
114 ### *2.1 Studied site*
115 The studied site is located on the Yonne plateau, France where Albeluvisol/Retisol (IUSS
116 Working Group WRB, 2007/ IUSS Working Group WRB, 2015) developed in Quaternary non-
117 calcareous loess deposited above Eocene clays (Baize and Voilliot, 1988). The soils have been
118 cultivated over the last 200 years and a subsurface drainage was installed during 16 years. The
119 soils form four horizons: a silty, brown ploughed surface horizon; a silty grey E-horizon; and

two horizons composed of a complex mixture of several soil volumes of distinctive colors (Figure 1). In the upper of these two horizons, called E&Bt-horizon hereafter, the most abundant volumes are silty and of a white-grey (10YR8/2 to 10YR7/1, called WG volumes hereafter) to pale-brown (10YR7/4, called PB volumes hereafter) color. In the lower horizon called Bt-horizon hereafter, there are clayey volumes of ochre color (10YR5/6 to 10YR5/8, called O volumes hereafter). Black concretions and impregnations occur (called B volumes hereafter) in the core of the ochre volumes, in both Bt- and E&Bt-horizons (Cornu et al., 2012a).

Bulk soil samples were collected from the different horizons at different distances along a 4-m trench dug perpendicularly to a drain. The different soil volumes were extracted from the E&Bt- and Bt-horizons (Figure 1). Their physical properties - mineralogical and chemical composition, abundance and morphology - were extensively characterized (e.g., Cornu et al., 2012 a, 2012b; Frison et al., 2009; Montagne et al., 2016, 2008). Further methodological details can be found in Montagne et al. (2008).

The soil profile 400 cm from the drain (P400) was shown to represent the Retisol differentiation with a negligible influence of the drain (Montagne et al., 2016, 2008), while differences observed between the soil profiles at 400 cm (P400) and 60 cm (P60) distance from the drain were interpreted as reflecting the impact of drainage on the soil, i.e., the effect of enhanced eluviation and a decline in reducing processes (Montagne et al., 2016). These two profiles were further characterized for Fe isotope measurements.

2.2 Sample preparation for Fe isotope analysis

For bulk soil and soil volume analyses, samples were dried at 40°C and sieved to <2 mm. For concentration and isotopic analyses, an aliquot of each sample was ground to fine powder using an agate mortar. For each sample, between 0.15 and 0.20 g of powdered soil was calcinated at 400°C for 4 hours in order to eliminate organic matter. Then, the samples were

dissolved in a mixture of concentrated HF-HNO_3, followed by concentrated HCl, at ~ 120-130°C, during 48 hours. After drying down, the samples were taken up in 7N HCl-0.001% H_2O_2 for Fe separation and purification. Iron was separated and purified by anion exchange chromatography using the AG MP1, 100-200 mesh, chloride form, according to the protocol of Maréchal et al. (1999). All reagents were ultrapure distilled or Seastar© quality and overall procedural blanks contained negligible quantities of Fe (< 15 ng) compared to the total dissolved sample Fe content. Yield (recovery) of the total liquid ion exchange resin chromatography procedure was verified and within 95 ± 5%. The reference material CCRMP Till-1 was analyzed with each batch of samples and Fe concentration analyses were in agreement with the certified values (± 0.1%).

2.3 Isotopic analyses

Iron isotope analyses were performed using MC-ICP-MS Neptune^{Plus} at CEREGE in medium-resolution. Prior to measurements, pure Fe fractions were diluted and doped with Cu (VWR ICPMS solution) to concentrations of 1 µg/g of both analytes which resulted in total Fe and Cu ion beams around 1:1. Iron (^{54}Fe, ^{56}Fe, ^{57}Fe and ^{58}Fe) and Cu (^{63}Cu and ^{65}Cu) isotopes were measured in wet plasma conditions using a thermoregulated spray chamber (Isomist from Glass expansion regulated at 10°C) and in multi-static mode (magnet jump alternating between Fe and Cu isotopes). The instrumental mass discrimination was corrected both via Cu isotopes and standard-sample-standard bracketing with IRMM-524a (also diluted and doped with Cu to match the concentration of the samples). Iron isotope results are reported relative to the IRMM-524a standard using the conventional δ notation, in ‰ (Eq. 1). Thus, $\delta^{56}Fe<0‰$ reflects enrichment in light ^{54}Fe isotopes, while $\delta^{56}Fe>0‰$ reflects enrichment in heavy ^{56}Fe isotopes (Eq. 1).

$$\delta^{56}Fe = [(^{56}Fe/^{54}Fe)_{sample} / {}^{56}Fe/^{54}Fe)_{IRMM524a} - 1]^{*}1000 \quad (1)$$

The analytical reproducibility (2SD) calculated on the basis of repeated measurements of the IRMM-524a standard was 0.07 and 0.11‰ (N=78) for $\delta^{56}Fe$ and $\delta^{57}Fe$, respectively. In a $\delta^{57}Fe$ vs. $\delta^{56}Fe$ diagram, all soil sample measurements plot along a line with a slope which is equal, within analytical error, to the theoretical value of ln(M57/M54)/ln(M56/M54)=1.48 (e.g., Beard and Johnson, 2004; Craddock and Dauphas, 2011), indicating mass-dependent fractionation and no influence of isobaric interferences. Data accuracy was monitored by repeated analyses of the rock standards with known Fe isotopic compositions, with each batch of samples.

2.4 Mass balance

We used the isotopic data together with the available information on Fe concentrations and volume abundances (Table 1) of Fe-bearing mineral phases in the individual volumes (Montagne et al., 2008) for the mass balance calculations.

At the scale of the horizon, we set up a similar mass balance to verify that the sum of volumes corresponds to the bulk soil (Eq. 2) and that no bias was introduced into the Fe isotopic compositions during the volume separation and analyses.

$$\delta^{56}Fe_{E\&Bt} = (\delta^{56}Fe_O \times Fe_O \times Ab_O + \delta^{56}Fe_B \times Fe_B \times Ab_B + \delta^{56}Fe_{PB} \times Fe_{PB} \times Ab_{PB} + \delta^{56}Fe_{WG} \times Fe_{WG} \times Ab_{WG}) / Fe_{E\&Bt} \quad (2)$$

where Fe stands for Fe concentration, $\delta^{56}Fe$ value for Fe isotopic compositions, Ab for the abundance of a given volume (% of the picture surface, Montagne et al., 2016), subscripts "O", "B", "PB" and "WG" for ochre, black, pale-brown and white-gray volumes, respectively, and "E&Bt" for the bulk $E\&Bt_{35\text{-}45\ cm}$ -horizon. The calculated $\delta^{56}Fe$ values were in agreement, within the analytical error with the analyzed $\delta^{56}Fe$ values.

Furthermore, the mass balance approach allowed us to estimate the isotopic compositions of the Fe fluxes (losses/gains) (i) at the scale of a horizon and (ii) among the volumes. These fluxes are considered to represent the Fe concentrations and the Fe isotopic signatures in the

195 solution resulting from the differentiation of the of the studied Retisol. The aim of this
196 calculation was to evaluate the fractionation of the entire process involving, on the one hand,
197 the dissolution of Fe-oxides, i.e. release of Fe into solution, and on the other hand, the
198 precipitation of Mn oxides containing Fe, i.e., removal of Fe from the solution.

199 We calculated Fe fluxes and their isotopic signatures linked to the studied Retisol
200 differentiation at a scale of horizons and among the soil volumes, using the Brimhall et al.
201 (1991) mass balance approach (Eq. 3), adapted for soil volumes by Montagne et al. (2008).

202 $$m_{Fe,\,flux} = 1/1000 \times (\rho_{reference} \times C_{Fe,\,reference} \times Th \times \tau_{Fe,\,product})/(\varepsilon_{imm,product} - 1) \quad (3)$$

203 where ρ corresponds to the bulk density in g cm^3, C to the concentration of Fe in g kg, Th to
204 the thickness of the horizon in cm, and ε and τ to strain and the open-system mass-transport
205 function, respectively, as defined by Brimhall et al. (1991). To compute these functions, quartz
206 was selected as the immobile element, subscript "imm" (Montage et al., 2008). The subscripts
207 "reference" and "product" refer to the soil volume taken as a reference, i.e., the parent material,
208 and to the product of the transformation, respectively. For example, at the scale of a horizon,
209 the flux of Fe lost at P400 was related to the natural differentiation of the $E\&Bt_{400}$ horizon from
210 the reference O volume while at P60, it was related to the differentiation of the $E\&Bt_{60}$ from
211 the reference $E\&Bt_{400,}$ due to the drainage. Furthermore, among the volumes, in the calculation
212 of the flux related to the reference O volume dissolution, the O volume is the reference while
213 B- and PB volumes are products of the transformation. In the calculation of the Fe flux linked
214 to the formation of the WG volume, the PB volume is the reference and the WG volume is the
215 product of the transformation.

216 Since the soil volumes consist of variations of proportions of different minerals (goethite,
217 ferrihydrite, Mn-oxide, clay minerals; Montagne et al., 2008) we used the mass balance
218 approach to calculate the theoretical $\delta^{56}Fe$ values of these mineral phases (Eq. 4):

219 $$\delta^{56}Fe_{Vol} = (\delta^{56}Fe_{Clay} \times Fe_{Clay} + \delta^{56}Fe_{FH} \times Fe_{FH} + \delta^{56}Fe_{GT} \times Fe_{GT} + \delta^{56}Fe_{MnOx} \times Fe_{MnOx})/Fe_{vol} \quad (4)$$

where the subscripts “Vol”, “Clay”, “FH”, “GT” and “MnOx” stand for the volume type, clay minerals, ferrihydrite, goethite and Mn oxides, respectively. Doing this for each volume, we obtained four equations. By solving this linear system, where $\delta^{56}Fe$ values of the four mineral phases (clay minerals, ferrihydrite, goethite and Mn oxides) were unknown, the theoretical $\delta^{56}Fe$ values for these minerals were determined.

3. RESULTS AND DISCUSSION

3.1 No Fe isotope fractionations in bulk soils but large isotopic contrasts between soil volumes

Iron concentrations in both soil profiles varied from 15.5 ± 0.8 to 26.4 ± 1.3 g kg^{-1} in P60 and from 16.1 to 27.4 ± 1.4 g kg^{-1} in P400 and showed an evolution with depth typical of Retisols, with the upper horizons, Ap and E&Bt, depleted in Fe compared to the deep Bt-horizons (Figure 2 a, b). This evolution was a result of clay translocation and subsequent strong bleaching due to the periodic saturation and reduction of iron compounds (e.g., Pedro et al, 1978). Bulk soil Fe isotopic compositions remained constant within the analytical error, close to $\delta^{56}Fe = 0 \pm 0.05‰$, throughout both soil profiles (Figure 2 c, d). These observations corroborate literature data on bulk soils, where a large range of Fe concentrations contrasts with minor isotopic variability (e.g., Emmanuel et al., 2005; Fantle and De Paolo, 2004; Fekiacova et al., 2017, 2013; Poitrasson et al., 2008; Wiederhold et al., 2007a, 2007b).

Contrasting with the absence of isotopic fractionation in the bulk soil samples along the soil profiles, the soil volumes sampled in the E&Bt-horizons were heterogeneous in both Fe concentrations (Figure 2 a, b) and isotopic compositions (Figure 2 c, d). Black (B) volumes were enriched in Fe (45 ± 2 g kg^{-1} and 33 ± 2 g kg^{-1} for B_{400} and B_{60}, respectively) compared to ochre (O) volumes (37 ± 2 g kg^{-1} and 33 ± 2 g kg^{-1} for O_{400} and O_{60}, respectively), while pale-brown (PB) and white-grey (WG) volumes were depleted in Fe (15 ± 0.7 g kg^{-1} and 12 ± 0.6 g kg^{-1} for PB_{400} and PB_{60}, respectively and 10 ± 0.5 g kg^{-1} and 8 ± 0.4 g kg^{-1} for WG_{400}

245 and WG_{60}, respectively), as already described in Montagne et al. (2008). Furthermore, B
246 volumes were enriched in light Fe isotopes (-0.49 ± 0.05‰ and -0.39 ± 0.05‰ for B_{400} and B_{60},
247 respectively), while WG volumes were enriched in heavy Fe isotopes (0.29 ± 0.06‰ and
248 0.15 ± 0.03‰ for WG_{400} and WG_{60}, respectively). These contrasts in Fe isotopic compositions
249 between individual soil volumes provide evidence of fractionating processes that occur during
250 the internal horizon differentiation. However, the resulting bulk soil isotopic signatures were
251 similar across horizons, which suggests, given that there is a loss of Fe from a horizon (for
252 $E\&Bt_{400}$: -0.65 g cm^{-2}; for $E\&Bt_{60}$: -0.57 g cm^{-2}), that the processes-related isotopic
253 fractionations compensate each other (directions and/or amplitudes) and generate a
254 homogenous integrated signal for a bulk soil sample, over the profile. This interpretation
255 corroborates the hypotheses proposed in the previously published literature to explain a bulk
256 soil Fe isotopic homogeneity (e.g., Wiederhold et al., 2007a, 2007b).
257
258 *3.2 Iron isotopic contrasts between soil volumes - evidence of internal horizon reorganization*
259 *during the Retisol differentiation (the P400 soil profile)*
260 At a distance of 400 cm from the drain, the O volume is characterized by high Fe
261 concentrations and δ^{56}Fe values close to 0‰ (Figure 3a), similar to the bulk δ^{56}Fe values. As
262 already mentioned above, the O volume corresponds to the initial Bt-horizon before
263 morphological degradation (Montagne et al., 2008). The PB and WG volumes, formed by
264 dissolution of the Fe oxides of the O volume (Montagne et al., 2008), have lower Fe
265 concentrations and higher δ^{56}Fe values (Figure 3a). Heavy δ^{56}Fe values in the Fe-poor soil
266 features have already been observed by Wiederhold et al. (2007b). Experimental dissolutions
267 of pure minerals showed that at the scale of a mineral, the heavy Fe-enriched residual phase
268 reflects a preferential removal of the light Fe isotopes during mineral dissolution. For example,
269 δ^{56}Fe values of up to -1.7‰ have been observed in the solution (e.g., Wiederhold et al., 2006).

Nevertheless, the studied soil volumes correspond to mixtures of several mineral phases (Montagne et al., 2008). We calculated Fe fluxes from the O to PB and PB to WG volumes and their Fe isotopic signatures were not significantly different from 0 ‰ (-0.02 ‰ and -0.03 ‰, for Fe flux from O and PB, respectively; Figure 4), suggesting no fractionation related to the dissolution of their Fe-oxides in these volumes. Thus, the heavy $\delta^{56}Fe$ values of the residual volumes (PB, WG) are likely to reflect the Fe isotopic signatures of the residual mineral phases (silicates). At the scale of soil volumes in these Retisols, we propose that the observed isotopic contrast may result from a selective removal of a particular mineral phase. Dissolution is the main process of morphological differentiation in this Retisol (Montagne et al., 2016) and this explanation is consistent with the $\delta^{56}Fe$ value close to 0‰ calculated for the total Fe lost during the transformation of the reference (parent) O volume to the $E\&Bt_{400}$ horizon ($\delta^{56}Fe$ = 0.06‰).

Furthermore, a light Fe pool is immobilized within the B volume by precipitation of Mn oxides containing Fe and of ferrihydrite, in the core of the remaining O volume. The B volumes formed have negative $\delta^{56}Fe$ values (-0.49 ± 0.05‰ and -0.39 ± 0.05‰ for B_{400} and B_{60}, respectively; Table 1). The precipitation of Mn oxides may be a fractionating process that preferentially incorporates light Fe isotopes in the solid phase. The calculated Fe flux with a negative $\delta^{56}Fe$ value (-2.94 ‰; Figure 4) corroborated this explanation. These results seem to contradict the isotopic theory (e.g., Bigeleisen and Mayer, 1947; Urey 1947) and experimental studies (e.g., Wiesli et al., 2004; Johnson et al., 2002; Skulan et al., 2002; Bullen et al., 2001), which predict that, at the scale of a mineral, heavy isotopes partition preferentially into a stronger bonding environment and during precipitation the heavy Fe isotopes are preferentially immobilized in the solid phase. However, in the soils, rapid precipitation with a dominant kinetic isotopic effect could explain the observed lighter isotopic signatures in the Mn oxides (e.g., Skulan et al., 2002).

294 The observed isotopic fractionations support the model of the internal mineralogical
295 reorganization of the E&Bt$_{400}$ horizon (Cornu et al., 2012a). Furthermore, these fractionations
296 are in agreement with the redox changes, which are dominant mechanisms controlling the
297 horizon evolution (Montagne et al., 2008). Lastly, despite the fact that light Fe flux is recorded
298 within the B volumes, its size is low and does not impact the global isotopic signature of the
299 flux and of the bulk soil at the horizon scale.
300
301 *3.3 Iron isotopic contrasts between soil volumes - evidence of enhanced morphological*
302 *degradation by eluviation induced by drainage*
303 From the E&Bt$_{400}$ to E&Bt$_{60}$ horizons, we also observed significant shifts of Fe
304 concentrations in the volumes (Figure 3b) due to the impact of the drain on the E&Bt-horizon
305 (Montagne et al., 2016). Iron concentrations decrease with decreasing distance from the drain
306 (Table 1). In contrast, we observed only small (PB and WG volumes) or non-significant, i.e.,
307 smaller than the analytical error (O and B volumes), isotopic differentiation with decreasing
308 distance from the drain (Table 1; Figure 3b). Thus, drainage, which has been shown to reduce
309 drastically reducing conditions and enhance eluviation close to the drain (Montagne et al.,
310 2016), results for Fe in a dominant physical mobilization that does not likely induce further Fe
311 isotope fractionations in soil volumes.
312
313 *3.4. Iron isotopic signatures of the mineral phases*
314 While physical separations of the minerals from the soil matrix are impossible, we can
315 calculate the theoretical δ^{56}Fe values for the main mineral phase of each volume (eq. 4). The
316 calculation suggested that goethite and ferrihydrite have δ^{56}Fe values close to 0‰, regardless
317 of the distance from the drain (Figure 5). This unfractionated isotopic signature is in agreement
318 with the calculated δ^{56}Fe values close to 0‰ of the Fe fluxes induced by their dissolution

(Figure 4). Both minerals represent the main Fe-bearing mineral phases of the ochre volume (Table 1), whatever the distance from the drain (Montagne et al., 2008), and thus fix the isotopic signature of this volume.

The Mn oxides containing Fe, which is the main mineral phase of the black volumes (Montagne et al. 2008), are markedly enriched in light Fe isotopes (-8.83 ‰ and -6.01 ‰ for Mn-ox$_{400}$ and Mn-ox$_{60}$, respectively; Figure 5). In contrast, the clay minerals, the main mineral phase of the WG volumes, have positive δ^{56}Fe values (1.31 ‰ and 0.60 ‰ for Clay$_{400}$ and Clay$_{60}$, respectively; Figure 5) indicating enrichment in heavy Fe isotopes. The δ^{56}Fe values of both Mn oxides and clay minerals differ significantly depending on the distance from the drain and the minerals from the farthest profile (P400) appear to be more strongly fractionated than the minerals from the profile close to the drain (P60) (Figure 5).

We propose two hypotheses to explain the calculated, less fractionated, Fe isotopic signatures of Mn oxides in the soil close to the drain (P60). First, decreasing isotopic fractionation with decreasing distance from the drain may reflect the progressive change in the dominant process controlling the mineralogy and Fe budget in these soils. While far from the drain (P400), dominant redox changes due to temporal water saturation remain active, this process disappears in the vicinity of the drain (P60). Since the redox process fractionates Fe isotopes, the larger isotopic fractionations observed at P400 may reflect the larger number of redox cycles experienced far from the drain (e.g., Schuth et al., 2015). However, we suggest that the fractionation observed between the volumes mostly results from precipitation rather than dissolution. Also, a higher abundance of B volumes at P60 compared to P400 indicated that the precipitation of Mn oxides occurs more in soils that are 60 cm rather than 400 cm from the drain (Montagne et al. 2008). This can be interpreted as precipitation of a younger generation of Mn oxides at P60, induced by drainage. Montagne et al. (2008) further hypothesized that the additional Mn input at P60 was partially due to dissolved elements

344 brought by lateral water flux from positions farther from the drain, and that Mn oxides
345 precipitated from the soil solution progressively. Such a progressive precipitation could induce
346 a progressive removal of light Fe isotopes from the soil solution by co-precipitation and/or
347 adsorption in the Mn oxides. However, this hypothesis needs to be verified, for example by
348 analyzing the Fe isotopic compositions of the soil solution at different distances from the drain.
349 Second, the source of Fe immobilized in the Mn oxides changes with decreasing distance
350 from the drain. It has been demonstrated that the Mn oxides form progressively by diffuse
351 impregnation of different volumes (Montagne et al., 2008; Stolt et al.,1994). At P400, the B
352 volumes form within the core of the O volume by precipitation of the light Fe released by
353 dissolution of Fe-oxides from the O volume. The Fe released by dissolution from the more
354 permeable PB volume (Frison et al., 2009), is lost from the horizon. In contrast, at P60 the
355 abundance of O volume decreased significantly thus the B volumes are more connected to the
356 PB volumes (Cornu et al., 2012a). Consequently, further development of the B volumes must
357 result from the Mn oxide precipitation with Fe originating from the dissolution of Fe from these
358 PB volumes. However, the dissolution of Fe oxides from the PB volumes also results in an Fe-
359 flux with an unfractionated δ^{56}Fe value (Figure 4). The flux of Fe originating from the PB
360 volumes has δ^{56}Fe values close to 0‰, as suggested by our mass balance calculation and should
361 not modify the δ^{56}Fe value of the precipitating Mn oxides. Thus, this second hypothesis cannot
362 explain the observed lower δ^{56}Fe values of Mn oxides in the soil close to the drain (P60).
363 Furthermore, the calculations predicted a shift of δ^{56}Fe values of the silicates from P400
364 towards P60 (Figure 5). The silicate fraction (i.e., particles <2µm, lutum) of these Retisols is
365 composed mostly of quartz, feldspars and clay minerals (i.e., kaolinite, illite, smectite and
366 chlorite). Quartz and feldspars do not contain Fe as a major element, but Fe can be present in
367 the clay minerals due to the substitution of Al and Mg. Cornu et al. (2012b) showed that the
368 proportions of different clay minerals changed with the distance from the drain, i.e., the

concentration of smectites decreased compared to the illite and interlayered clays. Furthermore, the presence of chlorites increased in the vicinity of the drain (Montagne et al. 2008). We hypothesized that the calculated shift in the $\delta^{56}Fe$ values from P400 to P60 may result from the selectivity of the eluviation process and reflects the described mineralogical changes in the proportions of different clay minerals. To verify this hypothesis, it would be necessary to analyze the Fe isotopic composition of the individual clay types. Such analyses could be partially achieved by particle size fractionation of the < 2 µm fraction (Hubert et al., 2012). Given that such a particle-size separation remains challenging due to the extremely small mineral size of the individual clays, verification of this hypothesis remains an open question for future research.

4. CONCLUSION

In this work we examined the Fe isotope fractionations related to processes occurring in a drainage-influenced sequence of Retisol, a soil type characterized by clay migration and the formation of redoximorphic features resulting from the strong Fe dynamics. We aimed at identifying (i) the Fe fluxes and their isotopic variability between soil horizons and between individual soil volumes and (ii) the isotopic signatures of the individual mineral phases, by combining the isotopic analyses, mineralogical data and mass balance calculation.

We showed that, as classically seen in the literature, the bulk soils have unfractionated Fe isotopic signatures, constant with depth, irrespective of the distance from the drain. However, the data on the different soil volumes suggest that some processes, and particularly precipitation, contributing to the internal horizon reorganization can produce large isotopic fractionations.

Furthermore, we shed light on the Fe isotopic compositions of the individual mineral phases present in the soil volumes, showing that clay minerals and newly precipitated Mn oxides

exhibit large isotopic fractionation. Our results suggest that while the residues of dissolution, represented by the morphologically degraded soil volumes, are rich in heavy Fe isotopes, the dissolution process associated with the reduction of Fe oxides is, in these Retisols, not a fractionating process. The apparent fractionation producing this heavy residue is likely to result from the selective removal of the Fe oxides, resulting in the accumulation of isotopically heavy clay minerals. In contrast, the process of Mn oxide precipitation incorporated light Fe isotopes. This last result appears to contradict the isotopic theory and remains to be explained. A dominant kinetic effect during rapid precipitation could explain the finding.

We suggest that further research should be directed towards better understanding the Fe isotopic fractionation by clay minerals and Mn oxides. Particle-size fractionation of clay minerals combined with sequential extractions should be performed in order to better constrain the isotopic signature of a single clay family. Spectroscopic approaches (Mössbauer, XAS, etc.) combined with laboratory experiments would help to shed light on the Fe isotopes fractionation during Mn oxide precipitation.

Acknowledgments

The authors wish to thank B. Angeletti for support with Q-ICPMS analyses. This research benefited from the support of the INRAE and of the EQUIPEX ASTER-CEREGE project. We also thank the reviewers for their constructive comments and suggestions, which have helped to improve this manuscript.

414 **REFERENCES**

415

416 Anbar, A. D. (2004) Iron stable isotopes: beyond biosignatures. Earth Planet. Sci. Lett. 217,
417 223–36.

418 Baize, D. and Voilliot, J.P., (1988). Notice de la carte des sols de l'Yonne à 1/50000, feuille
419 Joigny. Station agronomique de l'Yonne. Auxerre, France. 142 pp.

420 Balci, N., Bullen, T. D., Witte-Lien, K., Shanks, W. C., Motelica, M. and Mandernack, K. W.
421 (2006) Iron isotope fractionation during microbially stimulated Fe(II) oxidation and Fe(III)
422 precipitation. Geochimica et Cosmochimica Acta 70, 622–639.

423 Beard, B. L., Johnson, C. M., Cox, L., Nealson, K. H. and Aguilar, C. (1999) Iron isotope
424 biosignatures. Science 285, 1889-1892.

425 Beard, B. L. and Johnson, C. M. (2004) Reviews in Mineralogy & Geochemistry 10A Vol. 55,
426 319-357.

427 Bigeleisen, J. and Mayer, M. G. (1947) Calculation of equilibrium constants for isotopic
428 exchange reactions. The Journal of Chemical Physics 15(5), 261-267.

429 Borggaard, O. K. (1988) Phase identification by selective dissolution techniques. In : J. W.
430 Stucki et al. (eds.), Iron in Soils and Clay Minerals, 83-98.

431 Brantley, S., Liermann, L. and Bullen, T. D. (2001) Fractionation of Fe isotopes by soil
432 microbes and organic acids. Geology 29(6), 535-538.

433 Brimhall, G.H., Lewis, C.J., Ford, C., Bratt, J., Taylor, G. and Warin, O. (1991). Quantitative
434 geochemical approach to pedogenesis: importance of parent material reduction, volumetric
435 expansion, and eolian influx in lateritization. Geoderma 51 (1–4), 51–91.

436 Bullen, T. D., White, A. F., Childs, C. W., Vivit, D. V., Schulz and M. S. (2001) Demonstration
437 of significant abiotic iron isotope fractionation in nature. Geology 29(8), 699–702.

438 Chao, T. T. and Zhu, L. (1983) Extraction Techniques for Selective Dissolution of Amorphous
439 Iron Oxides from Soils and Sediments. Soil Sci. Soc. Am. J. 47, 225-232.
440 Cornell, R.M. and Schwertmann, U., (2003). The Iron Oxides. VCH, Weinheim, Germany.
441 573 pp.
442 Cornu, S., Montagne, D., Daroussin, J. and Cousin, I., (2012a) Image-analytically derived
443 conceptual model of Albeluvisol morphological degradation induced by artificial drainage
444 in France. Geoderma 189-190, 296-303.
445 Cornu, S., Montagne, D., Hubert, F., Barré, P. and Caner, L., (2012b). Evidence of short-term
446 clay evolution in soils under human impact C. R.Geoscience 344: 747–757
447 Craddock, P. R. and Dauphas, N. 2011 Iron isotopic compositions of geological reference
448 materials and chondrites. Geostandards and Geoanalytical Research 35(1), 101-123.
449 Emmanuel, S., Erel, Y., Matthews, A., Teutsch, N., (2005). A preliminary mixing model for Fe
450 isotopes in soils. Chem. Geol. 222, 23–34.
451 Fantle, M. S. and DePaolo, D. J., 2004. Iron isotopic fractionation during continental
452 weathering. Earth and Planetary Science Letters 228, 547–562
453 Fekiacova, Z., Pichat, S., Cornu, S. and Balesdent, J. (2013) Inferences from the vertical
454 distribution of Fe isotopic compositions on pedogenetic processes in soils. Geoderma 209-
455 210, 110-118.
456 Fekiacova, Z., Vermeire, M. L., Bechon, L., Cornelis, J. T. and Cornu, S. (2017) Can Fe isotope
457 fractionations trace the pedogenetic mechanisms involved in podzolization? Geoderma 296,
458 38-46.
459 Filgueiras, A. V., Lavilla, I. and Bendicho, C. (2002) Chemical sequential extraction for metal
460 partitioning in environmental solid samples. J. Environ. Monit., 2002, 4, 823-857.
461 Frison A., Cousin, I., Montagne, D., Cornu, S, (2009). Soil hydraulic properties in relation to
462 local rapid soil changes induced by field drainage: a case study. EJSS, 60: 662-670.

463 Guelke, M. and von Blanckeburg, F. (2007) Fractionation of Stable Iron Isotopes in Higher
464 Plants. Environ. Sci. Technol. 2007, 41, 1896-1901
465 Hubert, F., Caner, L., Meunier, A. and Ferrage, E. (2012) Unraveling complex < 2 mu M clay
466 mineralogy from soils using X-ray diffraction profile modeling on particle-size sub-
467 fractions: Implications for soil pedogenesis and reactivity. American Mineralogist 97(2-3),
468 384-398.
469 IUSS Working Group WRB (2007) World Reference Base for Soil Resources 2006, first update
470 2007. World Soil Resources Reports No. 103. FAO, Rome.
471 IUSS Working Group WRB (2015) World Reference Base for Soil Resources 2014, update
472 2015 International soil classification system for naming soils and creating legends for soil
473 maps. World Soil Resources Reports No. 106. FAO, Rome.
474 Icopini, G., A., Anbar, A. D., Ruebush, S. S., Tien, M. and Brantley, S. L. (2004) Iron isotope
475 fractionation during microbial reduction of iron: The importance of adsorption. Geology
476 32(3), 205–208.
477 Johnson, C. M., Skulan, J. L., Beard, B. L., Sun, H., Nealson, K. H. and Braterman, P. (2002)
478 Isotopic fractionation between Fe(III) and Fe(II) in aqueous solutions. Earth and Planetary
479 Science Letters 195, 141-153.
480 Kiczka, M., Wiederhold, J. G., Kraemer, S. M., Bourdon, B. and Kretzschmar, R. (2010) Iron
481 Isotope Fractionation during Fe Uptake and Translocation in Alpine Plants. Environ. Sci.
482 Technol. 44, 6144–6150.
483 Kusonwiriyawong, C, Bigalke, M., Abgottspona, F., Lazarov, M. Schuth, S. Weyer, S. and
484 Wilcke, W. (2017) Isotopic variation of dissolved and colloidal iron and copper in a
485 carbonatic floodplain soil after experimental flooding. Chemical Geology 459, 13–23.
486 La Force, M. J. and Fendorf, S. (2000). Solid-Phase Iron Characterization During Common
487 Selective Sequential Extractions. Soil Science Society of America Journal, 64(5), 1608.

488 Maréchal, C.N., Télouk, P., Albarède, F., (1999). Precise analysis of copper and zinc isotopic
489 compositions by plasma-source mass spectrometry. Chem. Geol. 156, 251–273.
490 Mathews, A., Zhu, X.-K. and O'Nions, K. (2001) Kinetic iron stable isotope fractionation
491 between iron (-II) and (-III) complexes in solution. Earth and Planetary Science Letters 192,
492 81-92.
493 Montagne, D., Cornu, S., Le Forestier, L., Hardy, M., Josière, O., Caner, L. Cousin, I.. (2008).
494 Impact of drainage on soil-forming mechanisms in a French Albeluvisol: input of
495 mineralogical data in mass-balance modelling. Geoderma, 145, 426–438.
496 Montagne D., Cousin, I., Cornu, S., 2016. Changes in the pathway and the intensity of albic
497 material genesis: Role of agricultural practices. Geoderma, 268, 156–164
498 Pedro, G., Jamagne, M. and Begon, J. C. (1978) Two routes in genesis of strongly differentiated
499 acid soils under humid, cool-temperate conditions. Geoderma, 20, 173-189.
500 Poitrasson, F., Viers, J., Martin, F., Braun, J. J., (2008). Limited iron isotope variation in recent
501 lateritic soils from Nsimi, Cameroon: implications for the global Fe geochemical cycle.
502 Chem. Geol. 253, 54–63.
503 Schuth, S., Hurraß, J., Münker, C. and Mansfeldt, T. (2015) Redox-dependent fractionation of
504 iron isotopes in suspensions of a groundwater-influenced soil. Chemical Geology 392, 74-
505 86.
506 Schwertmann, U (1991) Solubility and dissolution of iron oxides. Plant and Soil 130, 1-25.
507 Skulan, J. L., Beard, B. L. and Johnson, C. M. (2002) Kinetic and equilibrium Fe isotope
508 fractionation between aqueous Fe(III) and hematite. Geochimica et Cosmochimica Acta,
509 Vol. 66 (17), 2995–3015.
510 Stolt, M. H., Ogg, C. M. and Baker, J. C. (1994) Strongly contrasting redoximorphic patterns
511 in Virginia valley and ridge paleosols. Soil Sci. Soc. Am. J. 58, 477-484.

512 Thompson, A., Ruiz, J., Chadwick, O.A., Titus, M., Chorover, J., (2007). Rayleigh
513 fractionation of iron isotopes during pedogenesis along a climatic sequence of Hawaiian
514 basalts. Chem. Geol. 238, 72–83.
515 Urey H. C. (1947) The thermodynamic properties of isotopic substances. J. Chem. Soc.
516 (London). 562–581.
517 Wiederhold, J.G., Kraemer, M., Teutsch, N., Borer, P.L., Halliday, A.N., Kretzschmar, R.,
518 (2006). Iron isotope fractionation during proton-controlled and reductive dissolution of
519 goethite. Environmental Science & Technology 40, 3787–3793.
520 Wiederhold, J.G., Teutsch, N., Kraemer, M., Halliday, A.N., Kretzschmar, R., (2007a). Iron
521 isotope fractionation in oxic soils by mineral weathering and podzolization. Geochim.
522 Cosmochim. Acta 71, 5821-5833.
523 Wiederhold, J.G., Teutsch, N., Kraemer, M., Halliday, A.N., Kretzschmar, R., (2007b). Iron
524 isotope fractionation during pedogenesis in redoximorphic soils. Soil Sci. Soc. Am. J. 71,
525 1840–1850.
526 Wiesli, R. A, Beard, B. L. and Johnson, C. M. (2004) Experimental determination of Fe isotope
527 fractionation between aqueous Fe(II), siderite and “green rust” in abiotic systems. Chemical
528 Geology 211, 343–362.
529

Table and figure captions

Table 1:

Iron concentrations and isotopic compositions of the bulk soils and individual volumes.

Figure 1:

a) The different soil volumes of the E&Bt-horizon (photo from Cornu et al., 2012b) and corresponding colors used in the conceptual model. Ochre volume (O volume) corresponds to the parental material. Pale-brown volume (PB volume) formed by morphological degradation, i.e., dissolution of Fe-oxides, from the O volume. Further degradation, i.e., dissolution of Fe-oxides of the PB volume, produces white-grey volumes (WG volumes). Black volumes (B volumes) form by precipitation of the Fe and Mn released from this dissolution.

b) Conceptual model of the internal horizon reorganization (after Cornu et al., 2012b) representing differentiation of the parental O volume (Bt-horizon) into E&Bt-horizon at the positions P400 and P60. Abbreviations: O=ochre volume, PB=pale-brown volume, WG=white-grey volume, B=black volume, P400 and P60 correspond to positions 400 cm and 60 cm from the drain, respectively.

Figure 2:

Evolution with depth of Fe concentrations (a, b) and Fe isotopic compositions (c, d) in the Retisol profiles at different distances from the drain, 400 cm (a, c) and 60 cm (b, d).

Ap, E&Bt, Bt correspond to the horizons, O, B, PB, WG to the soil volumes. The analytical error of the Fe concentration analyses is ± 5%. The analytical error of the δ^{56}Fe values is 2SD calculated from the repeated analyses of the same sample solution. P400 and P60 correspond to positions 400 cm and 60 cm from the drain, respectively.

555

556 **Figure 3**:

557 Relationship between Fe concentrations and $\delta^{56}Fe$ values of the individual volumes 400 cm (a)
558 and 60 cm (b) from the drain. (a) Black arrows indicate Fe isotopes fractionation associated
559 with dissolution and precipitation. (b) Red arrows indicate the shifts in Fe concentrations and
560 $\delta^{56}Fe$ values with decreasing distance from the drain.

561

562 **Figure 4**:

563 Conceptual model of Fe fluxes during Retisol differentiation, i.e., during the transformation
564 from the reference O volume (parent material of E&Bt) to the E&Bt horizon, 400 cm from the
565 drain. O, PB, WG and B correspond to ochre, pale-brown, white-grey and black volumes,
566 respectively, 400 cm from the drain. Data within the rectangles correspond to the analyzed Fe
567 concentrations (Montagne et al. 2008), Fe isotopic compositions (this work) and calculated Fe
568 stock in the actual volumes, in the E&Bt-horizon, 400 cm from the drain. Data with arrows
569 represent the calculated Fe concentration and its $\delta^{56}Fe$ values in the Fe fluxes related to the
570 transformations between the volumes. Positive values (red font) = gains, negative values (blue
571 font) = losses. "F" corresponds to the fractional contribution of each volume.

572

573 **Figure 5**:

574 Theoretical $\delta^{56}Fe$ values calculated (Eq. 4) for the individual mineral phases present in the soil
575 volumes. P400 and P60 correspond to positions 400 cm and 60 cm from the drain, respectively.
576 Data on the Fe content in the mineral phases extracted during the different steps of sequential
577 extraction are from Montagne, 2006.

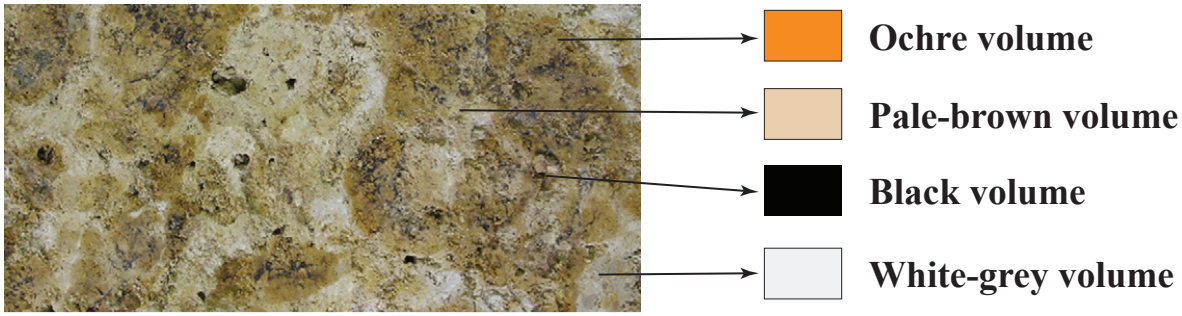
Ochre volume
Pale-brown volume
Black volume
White-grey volume

a)

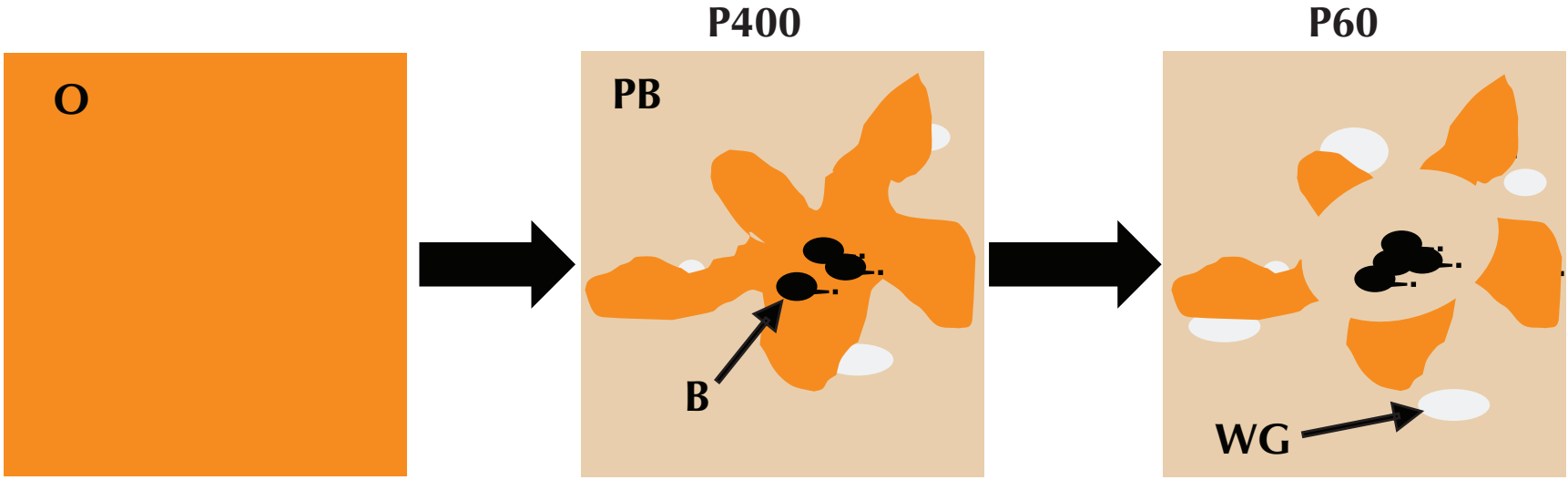
P400
P60
O
PB
B
WG

b)

Figure 1

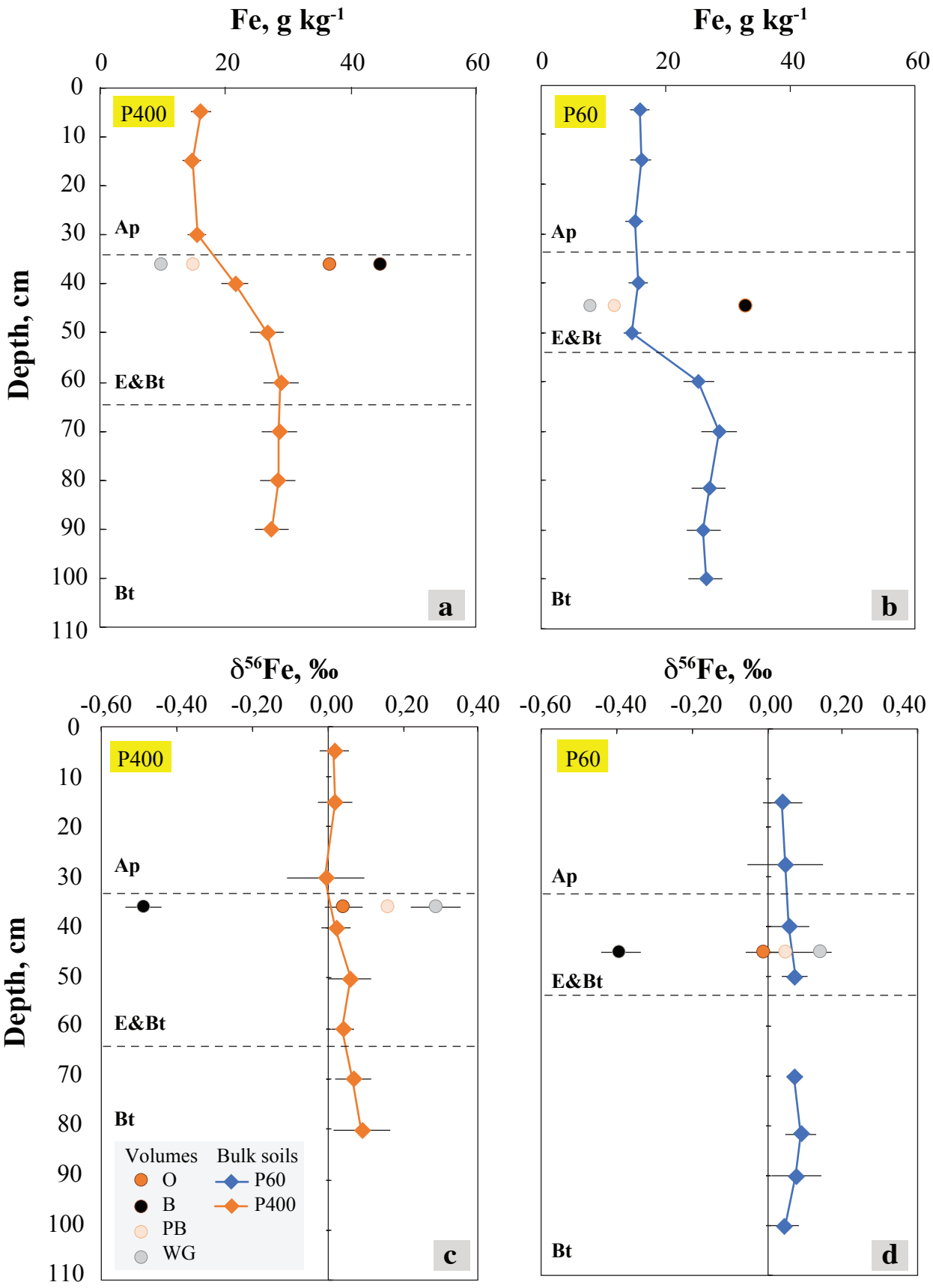
Fe, g kg-1
0
20
40
60
Depth, cm
0
10
20
30
40
50
60
70
80
90
100
110
P400
Ap
E&Bt
Bt
a
P60
b
δ56Fe, ‰
-0,60
-0,40
-0,20
0,00
0,20
0,40
c
d
Volumes
O
B
PB
WG
Bulk soils
P60
P400

Figure 2

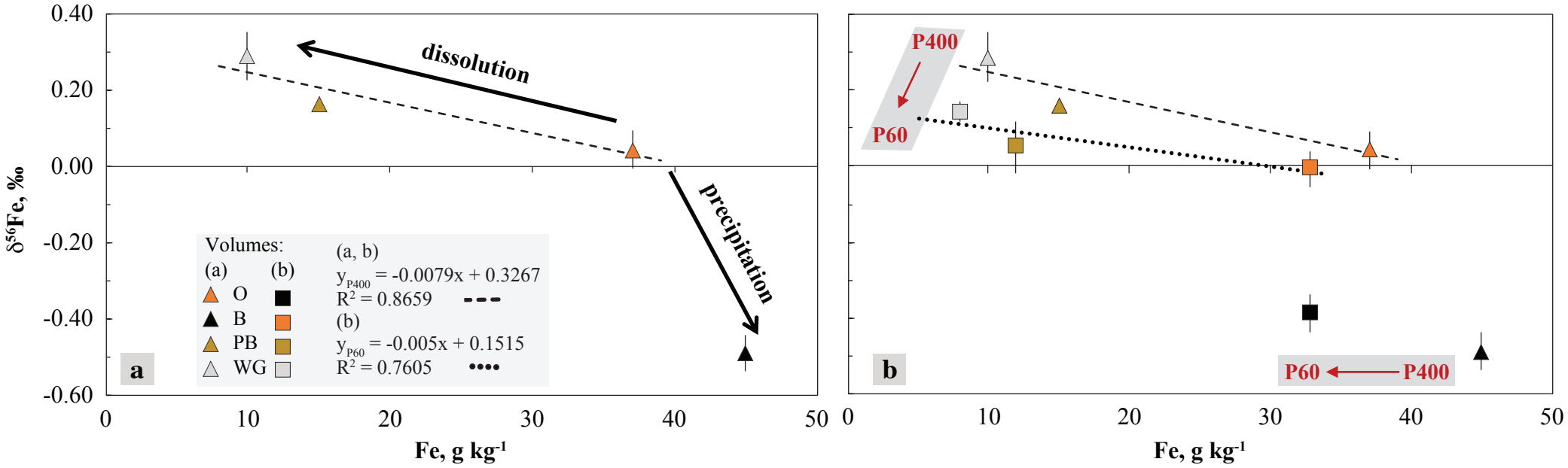
0.40
0.20
0.00
-0.20
-0.40
-0.60
δ56Fe, ‰
dissolution
precipitation
Volumes:
(a) (b)
O
B
PB
WG
(a, b)
yP400 = -0.0079x + 0.3267
R2 = 0.8659
(b)
yP60 = -0.005x + 0.1515
R2 = 0.7605
a
0
10
20
30
40
50
Fe, g kg-1
P400
P60
b
P60 ← P400
0
10
20
30
40
50
Fe, g kg-1

Figure 3

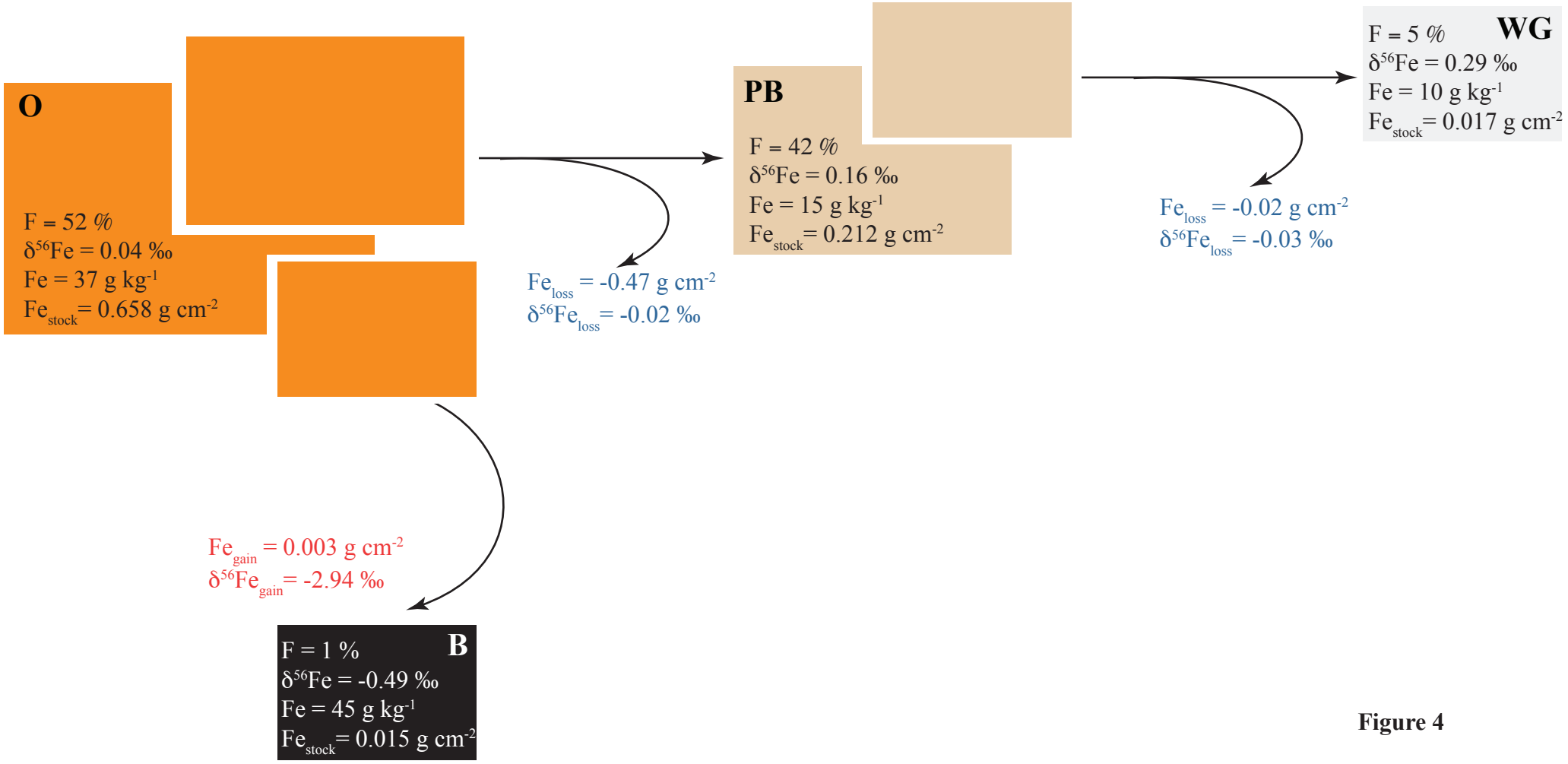
O
F = 52 %
δ56Fe = 0.04 ‰
Fe = 37 g kg-1
Festock = 0.658 g cm-2
Feloss = -0.47 g cm-2
δ56Feloss = -0.02 ‰
PB
F = 42 %
δ56Fe = 0.16 ‰
Fe = 15 g kg-1
Festock = 0.212 g cm-2
Feloss = -0.02 g cm-2
δ56Feloss = -0.03 ‰
WG
F = 5 %
δ56Fe = 0.29 ‰
Fe = 10 g kg-1
Festock = 0.017 g cm-2
Fegain = 0.003 g cm-2
δ56Fegain = -2.94 ‰
B
F = 1 %
δ56Fe = -0.49 ‰
Fe = 45 g kg-1
Festock = 0.015 g cm-2

Figure 4

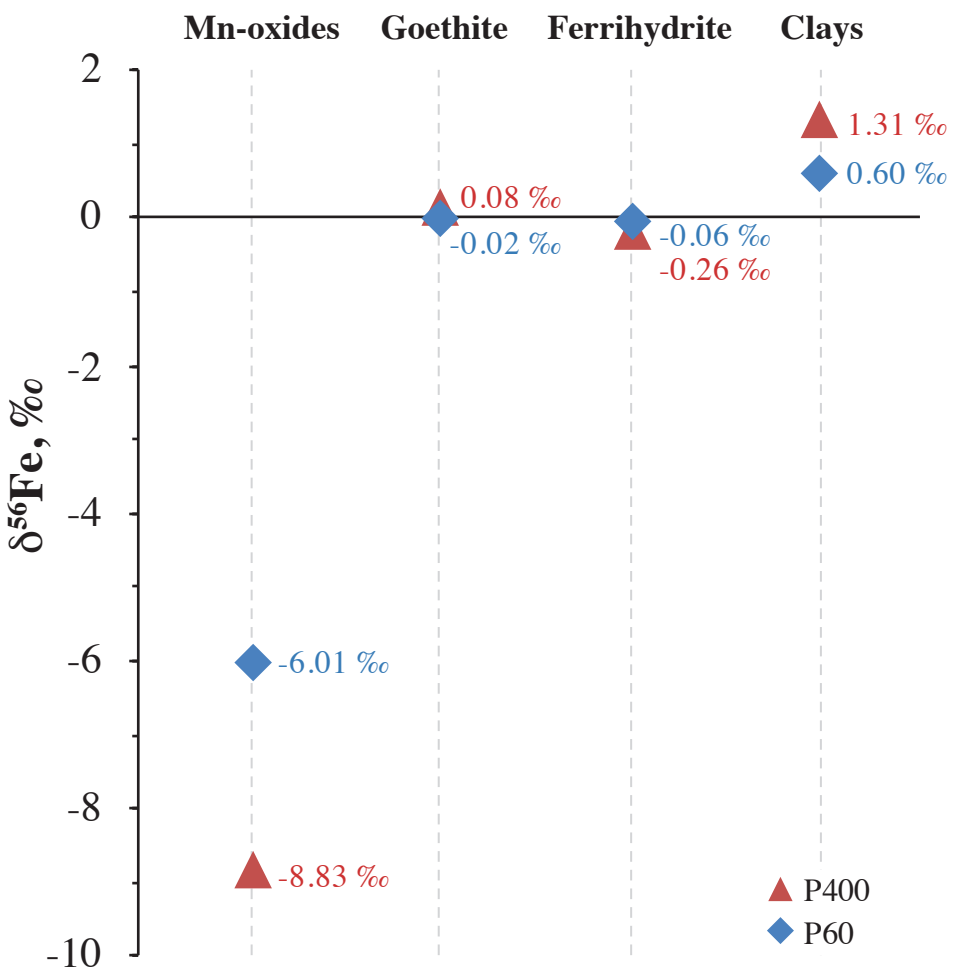
Mn-oxides
Goethite
Ferrihydrite
Clays
2
0
-2
-4
-6
-8
-10
δ56Fe, ‰
1.31 ‰
0.60 ‰
0.08 ‰
-0.02 ‰
-0.06 ‰
-0.26 ‰
-6.01 ‰
-8.83 ‰
P400
P60

Figure 5

Distance from drain	Horizon	Sample name	Depth, cm	Fe, g kg^{-1}*	δ^{56}Fe, ‰	2SD	Relative abundance, %*
Bulk soils							
60 cm	Ap	BB2A 0-10	0	15.9	na		
		BB2A 10-20	10	16	0.04	0.05	
	E	BB2A 20-35	20	15	0.05	0.10	
	E&Bt	BB2A 35-45	35	15.6	0.06	0.06	
		BB2A 45-55	45	14.7	0.07	0.03	
	Bt	BB2A 55-65	55	25.3	na		
		BB2A 65-75	65	28.5	0.07	0.02	
		BB2A 78-85	75	26.9	0.09	0.04	
		BB2A 85-95	85	26.1	0.08	0.07	
		BB2A 95-105	95	26.4	0.05	0.04	
400 cm	Ap	BB3D 0-10	0	16.1	0.02	0.04	
		BB3D 10-20	10	14.7	0.02	0.05	
	E	BB3D 25-35	25	15.5	-0.01	0.10	
	E&Bt	BB3D 35-45	35	21.6	0.02	0.04	
		BB3D 45-55	45	26.7	0.06	0.06	
		BB3D 55-65	55	28.9	0.04	0.03	
	Bt	BB3D 65-75	65	28.6	0.07	0.05	
		BB3D 75-85	75	28.4	0.09	0.07	
		BB3D 85-95	85	27.4	na		
Pedological volumes							
60 cm	E&Bt	White-grey	45	8	0.15	0.03	11 ±5
	(41-53 cm)	Pale-brown	45	12	0.05	0.07	55 ±6
		Ochre	45	33	-0.01	0.05	24 ±11
		Black	45	33	-0.39	0.05	10 ±3
400 cm	E&Bt						
	(32-44 cm)	White-grey	36	10	0.29	0.06	5 ±2
		Pale-brown	36	15	0.16	0.02	42 ±9
		Ochre	36	37	0.04	0.05	52 ±8
		Black	36	45	-0.49	0.05	1 ±1

* data from Montagne et al., 2008

Analytical errors for Fe concentrations equals to 5 %. Volume abundances are relative abundances of the different volumes in % of the picture surface (Montagne et al., 2016)

na - not analysed

Table 1